CHEMISTRY OF MATERIALS
Cite This: Chem. Mater. 2017, 29, 10122−10129
Article
pubs.acs.org/cm

Oxidation and Luminescence Quenching of Europium in $BaMgAl_{10}O_{17}$ Blue Phosphors

Lucia Amidani,*[,†] Katleen Korthout,[‡] Jonas J. Joos,[‡] Marte van der Linden,[§,†] Heleen F. Sijbom,[‡] Andries Meijerink,[∥] Dirk Poelman,[‡] Philippe F. Smet,*[,‡] and Pieter Glatzel*[,†]

[†]European Synchrotron Radiation Facility, 71 avenue des Martyrs, CS 40220, 38043 Grenoble, France

[‡]Lumilab, Department of Solid State Sciences, Ghent University, Krijgslaan 281 (S1), 9000 Ghent, Belgium

[§]Inorganic Chemistry and Catalysis, Debye Institute for Nanomaterials Science, Utrecht University, Universiteitslaan 99, 3584 CG Utrecht, The Netherlands

[∥]Condensed Matter and Interfaces, Debye Institute for Nanomaterials Science, Utrecht University, Princetonplein 5, 3584 CC Utrecht, The Netherlands

ABSTRACT: The efficient blue luminescence of Eu^{2+} doped $BaMgAl_{10}O_{17}$ is well-known to be severely degraded by prolonged irradiation with vacuum-ultraviolet light. The degradation process at the atomic level is however not fully understood. In this work we employed X-rays as an equivalent but accelerated cause of degradation, as an excitation source of luminescence and as an element-selective probe of both dopants and host-lattice chemical species. The X-ray absorption near edge structure (XANES) recorded in high energy resolution mode reveals that the structural properties of the host lattice are preserved during irradiation, while Eu^{2+} is rapidly oxidized. The correlation between Eu oxidation as derived from XANES and the decrease of blue luminescence is however not linear and a significant fraction of Eu^{2+} survives degradation, implying additional mechanisms for the quenching of the luminescence. Defects created during the photogeneration may reduce the ability of the remaining Eu^{2+} to receive or to radiatively release energy. A kinetic Monte Carlo simulation confirms that defects in the vicinity of a photogenerated Eu^{3+} can act as killer centers for the remaining Eu^{2+} and explain the observed accelerated quenching of the blue luminescence. The present approach, which takes full advantage of the different interactions of X-ray radiation with impurity doped luminescent materials, can easily be transferred to reveal degradation pathways in other phosphors.

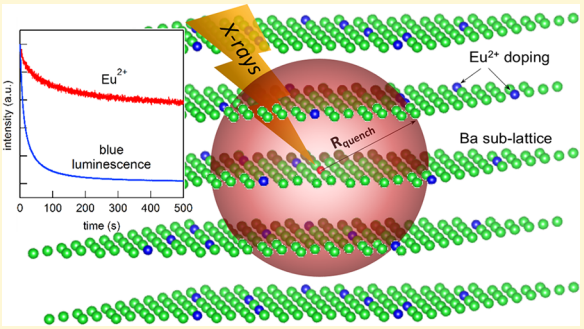

INTRODUCTION

Europium doped Barium Magnesium Aluminate, $BaMgAl_{10}O_{17}$:Eu (BAM:Eu), is a well-known blue phosphor with excellent performance. It is extensively applied as the blue component in technological applications as Plasma Display Panels (PDP) and fluorescence light bulbs,[1−3] and it was the object of renewed interest due to its possible application in near-UV pumped white LEDs.[4−9] The emission of BAM:Eu consists of a broad band centered at 450 nm arising from the interconfigurational transition of Eu^{2+} from the $4f^65d^1$ excited state to the $4f^7$ ground state. Both excitation and emission are electric dipole allowed, yielding strong absorption and fast decay (τ = 800 ns).[10] The quantum efficiency reported for excitation with UV and vacuum-ultraviolet (VUV) radiation is close to unity.[11] Despite the outstanding luminescent properties, BAM:Eu is also known for its easy degradation during annealing,[12−14] even at moderate temperature (400 °C), and during prolonged irradiation with VUV light.[15−17] Annealing treatments are often part of the deposition process of thin phosphor layers, while deep VUV plasma discharge (147 nm) from Xe/Ne gas mixtures are used to excite the phosphor. Exploitation of BAM:Eu for technological applications is therefore hindered by its poor stability and understanding the modifications that correlate with damage at the atomic level is necessary to find viable routes to improve the material. The methodology presented in this work can directly be transferred to other phosphors showing reduced stability, such as many sulfides or nitrides.[18]

$BaMgAl_{10}O_{17}$ crystallizes in the β-alumina structure characterized by $MgAl_{10}O_{16}$ units densely packed in spinel blocks and intercalated by poorly occupied planes of Ba−O units (Figure 1).[19] The stiffness of the spinel blocks contrasts with the loose bonds of Ba−O planes that exhibit high cation mobility and can thus act as ion conduction layers (CL). To turn BAM into a phosphor, Eu^{2+} substitutes Ba^{2+} in the CL. Ba^{2+} has a large coordination sphere composed of nine O and because Eu^{2+} has a smaller ionic radius, it may not fully remain at the Ba site and can occupy empty sites available in the CL. BAM can also be

Received: September 15, 2017
Revised: November 9, 2017
Published: November 17, 2017

DOI: 10.1021/acs.chemmater.7b03918
Chem. Mater. 2017, 29, 10122−10129

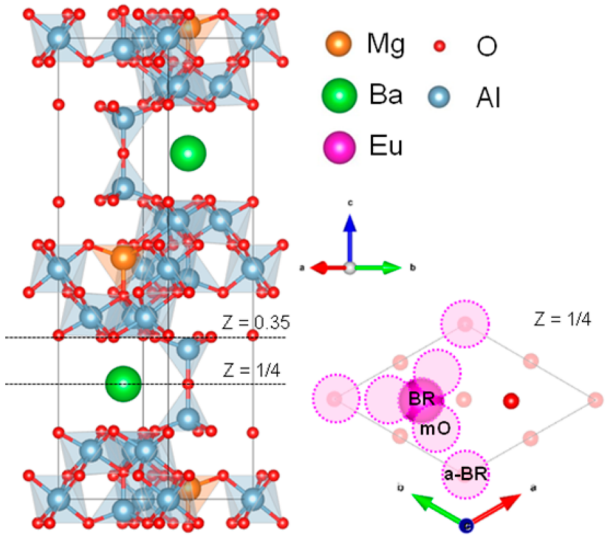

Figure 1. Left: unit cell of $BaMgAl_{10}O_{17}$. Spinel blocks are intercalated by conduction layers containing a Ba atom and a bridging O. Right: cut of the $Z = 1/4$ showing Eu at a Beaver-Ross (BR) site (pink) and the bridging O (red). Light pink circles indicate mO and a-BR sites to where Eu is supposed to migrate. Oxygen atoms lying on the plane $Z = 0.35$ are shown in light red.

doped or codoped with Mn^{2+} to obtain a green phosphor.[20] Mn^{2+} preferentially substitutes Mg^{2+} in the spinel block because of the similar ionic radii.

Degradation of BAM:Eu by VUV results in a reduced intensity of the emitted light accompanied by a color shift to longer wavelengths and a broadening of the emission band.[16,21] The origin of BAM:Eu degradation has been investigated at length in the attempt to find synthesis routes and strategies to preserve the phosphor quality over time. While it is generally agreed that degradation during annealing in air is caused by oxidation of Eu^{2+},[13] less consensus is found about the origin of VUV induced damage. The photoluminescence process upon VUV irradiation is the result of three main steps: absorption of light from the excitation source, transfer of the energy to the luminescent impurities and radiative de-excitation of Eu^{2+}. VUV irradiation may affect one or several of the following mechanisms: structural changes of the host lattice may alter the absorption properties of the host matrix and photogeneration of defects may favor nonradiative recombination that prevents the energy to be transferred to the impurities. VUV can also act on the luminescent centers directly by promoting oxidation of Eu^{2+} or by inducing Eu atoms to displace from the original site. Experimental evidence for increased density of defects,[10,22,23] Eu^{2+} oxidation,[24,25] and Eu displacement,[15,16] was reported for BAM:Eu degraded by VUV radiation and each identified as the primary source of degradation. However, the role these processes play in the decrease of luminescence brightness remains elusive and a clear picture of the degradation from VUV irradiation is still missing.

In this work we present an original approach to study BAM degradation based on X-ray Absorption Spectroscopy (XAS) and the simultaneous collection of radio-luminescence (RL) spectra. We exploited X-rays in three ways, as (1) an excitation source for RL, (2) an intense source of radiation that induces damage, and (3) an element-selective and chemically sensitive probe of the local atomic and electronic structure. This approach allows for simultaneous monitoring of luminescence, electronic, and structural changes while the damage occurs. We separately probed the structure of the conduction layer and the spinel block by looking at Eu, Ba, and Mn with High Energy Resolution Fluorescence Detected (HERFD)-XANES. Spectra with increasing X-ray dose and thus increasing degradation were recorded on the different chemical species, and RL was simultaneously collected to monitor the status of luminescence behavior.

We found that the host matrix is stable while a large fraction of Eu^{2+} impurities are rapidly oxidized to Eu^{3+}. The analysis of the time scales for Eu oxidation and RL decrease suggests that the disappearance of part of the emitting centers is not sufficient to account for the fast RL decay and that the creation of defect centers in proximity of Eu^{3+} can also be involved in luminescence quenching. A Monte Carlo simulation confirms that this model can account for the observed dynamics.

EXPERIMENTAL SECTION

The samples measured were commercially available powders of Eu-doped BAM and Eu, Mn codoped BAM. XRD measurements indicate that both powders are single phase. The average crystallite size measured with SEM is 5 μm for BAM:Eu and between 5 and 10 μm for BAM:Eu,Mn. The dopants' atomic concentrations were estimated from EDX data. The Eu concentration relative to all Ba plus Eu atoms is 7% in BAM:Eu and 15% in BAM:Eu,Mn and the Mn concentration relative to all Mg plus Mn is 31%.

Pellets for X-ray measurements were prepared by mixing 5−10 mg of phosphor powder with 50 mg of cellulose. HERFD-XANES at the Eu and Ba L_3-edge and at Mn K-edge were taken on the ID26 beamline at the ESRF.[26] Compared to conventional fluorescence detected XANES which integrates the full characteristic fluorescence line, HERFD-XANES spectra are obtained by integrating only a small energy bandwidth centered on the maximum of the characteristic X-ray fluorescence emitted by the chemical species under investigation. The integrated bandwidth, typically of the order of 1 eV, is smaller than the core-hole lifetime broadening resulting in a sharpening of XANES features.[27] A spectrometer based on Bragg optics in Rowland geometry was used to analyze the emitted X-rays. In all our measurements the incident beam energy was selected by means of a Si(311) double crystal monochromator while the spectrometer was equipped with a set of five Ge(333) analyzers to record Eu L_3- and Mn K-edge and two Ge(400) to record Ba L_3-edge HERFD-XANES. The $L\alpha_1$ fluorescence channel was monitored for the L_3-edges (5844.7 eV for Eu and 4466.5 eV for Ba) while the $K\alpha$ fluorescence was recorded for the Mn K-edge (4465.6 eV). The overall (incoming and emitted) energy bandwidth selected for Mn and Eu measurements was 0.8 and 0.5 eV for Ba.

To collect the RL emitted during irradiation, the sample stage was equipped with a UV−visible spectrometer (Maya2000pro, Ocean Optics) coupled with an optical fiber aligned to the spot were X-rays hit the sample. The spectrometer was not calibrated for the spectral sensitivity. To simultaneously measure the X-ray effect on RL and on Eu^{2+}, we fixed the incident energy to the maximum of the Eu^{2+} absorption peak, irradiated a spot of the pellet for 2500 s while sampling the X-ray fluorescence intensity of the Eu^{2+} signal every 150 ms. Simultaneously we acquired a UV−visible emission spectrum every 150 ms for the full duration of the irradiation. The same measurement was performed at Ba L_3-edge. To characterize the progressive damage with XANES we set the scanning time to 5 s and acquired a series of XANES on the same spot before moving to a fresh spot and repeating the acquisition. Spectra from several spots and identical irradiation time were averaged to reach the desired spectral quality. The first spectrum of the cycle is the HERFD-XANES of the sample as fresh as we can measure it. Approximately 1 s is needed to scan the pre-edge region and 1 s to scan the edge region, meaning that the edge region of the first XANES is representative of a sample irradiated for 2 s. All spectra were normalized to the incoming photon flux and the X-ray beam footprint on the sample was 0.5 × 0.075 mm^2

DOI: 10.1021/acs.chemmater.7b03918
Chem. Mater. 2017, 29, 10122−10129

(horizontal × vertical). The total X-ray flux was approximately 10^{12} photons/second.

A pellet made of 10 mg of BAM:Eu and 80 mg of boron nitride was prepared and mounted in a furnace adapted for X-ray in situ studies. Three spots of the pellet were used to measure three XANES of 5 s before the degradation, then the same three spots and a fourth one were irradiated for 300 s by the X-ray beam. After X-ray degradation, a continuous flow of 4% H_2/He gas mixture regulated by a mass flow controller was allowed in the sample space. The furnace was programmed to ramp the temperature from RT to 1000 °C at a rate of 5 °C/min. During the annealing, one of the degraded spots was used to monitor the intensity of the Eu^{2+} peak every 5 min, and it was found that the initial intensity of Eu^{2+} peak was recovered at 630 °C; XANES spectra were collected on the previously damaged spots.

RESULTS

Figure 2 shows a selection of BAM:Eu RL spectra acquired during the 2500 s irradiation with the incident X-rays tuned to the Eu L_3-edge maximum. The spectrum is dominated by a broad band centered at 453 nm corresponding to the characteristic blue emission. At longer wavelengths we resolve a shoulder centered at 616 nm that is not reported in literature. The insets show the long wavelength region of the selection of RL spectra (bottom) and of the image obtained with all RL spectra collected in the first 30 s (top). The intensity of the shoulder at 616 nm relative to the main band increases in the first 3 s, after which it decreases at the same rate as the main band. In the same wavelength range, a somewhat similar feature was observed in a study dedicated to BAM:Eu irradiation with X-rays and electron bombardment[28] and was associated with Eu^{3+}. At 693 nm we indeed observe a sharp line consistent with the $^5D_0$–$^7F_4$ transition in Eu^{3+}. Although part of this emission might be related to Mn^{4+} impurities, the telltale traces of other Eu^{3+} lines, especially $^5D_0$–$^7F_2$, can be discerned by subtracting the tail of the main band and the shoulder at 616 nm from the data (not shown), confirming the presence of luminescent Eu^{3+}. Differently from the unexplained shoulder, the intensity of the $^5D_0$–$^7F_4$ line relative to the main band is stable ruling out that they have a common origin. However, neither of the features evolves with irradiation according to the increase of Eu^{3+} concentration observed with XANES, as will be shown in the following. We conclude that the $^5D_0$–$^7F_4$ line is not representative of all the Eu^{3+} incorporated in the sample. Further investigation is needed to clarify the nature of the broad shoulder at 616 nm which may be associated with a very early stage of the degradation process like the generation of defects involved in Eu^{2+} oxidation.

Irradiation causes a decrease of the intensity of the main band and it also affects the spectral shape. Figure 3 shows the selection of spectra of Figure 2 normalized to maximum intensity. For long irradiation times of 1000 s, the Eu $^5D_0$ – $^7F_2$ transition around 616 nm becomes visible, although the contribution to the total RL emission intensity is very limited. Progressive irradiation causes a redshift and a broadening of the main band. The variation of the integrated intensity, the position of the maximum, and the fwhm extracted from each RL spectrum are shown as a function of irradiation time in the insets. All figures reach a stable value after 1000 s. RL intensity is reduced to 1% of the initial value, the maximum of the emission peak is red-shifted by 4 nm and the fwhm is increased by almost 4 nm. These effects are in agreement with what was reported for VUV damage on BAM:Eu[15,16,22,29] and confirm that X-rays and VUV induce an analogous degradation.[24,28] We notice that while a temperature increase due to prolonged X-ray irradiation would result in a broadening of the main band,[30] only an atomic structural change can explain the redshift. The

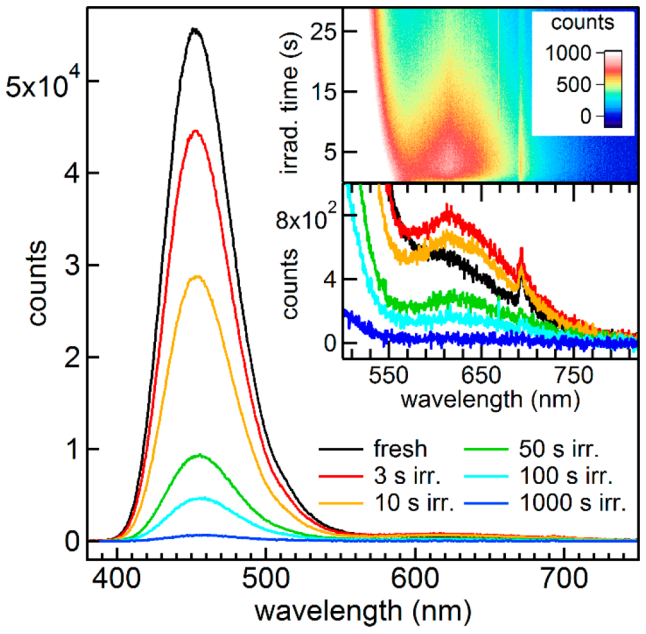

Figure 2. Evolution of the RL of BAM:Eu during X-ray irradiation. Main panel: full emission spectra at selected stages of irradiation. Bottom inset: magnification of the long wavelength region showing the broad shoulder at 616 nm and the line at 693 nm associated with Eu^{3+}. Top inset: contour plot obtained with all measured RL spectra showing the evolution of long wavelength region during the first 30 s of irradiation.

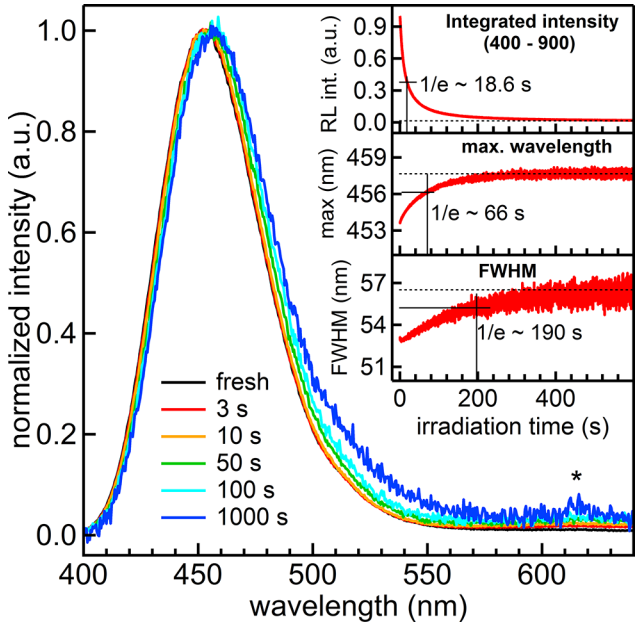

Figure 3. Selection of RL spectra of BAM:Eu normalized to the maximum. The three insets show the evolution as a function of irradiation of (from top to bottom): the normalized integrated intensity of main band, the position of maximum and the fwhm. Each inset reports a straight line indicating the value reached at full degradation (1000 s) and the time needed to achieve 63% of the full variation range. The asterisk indicates the $^5D_0$–$^7F_2$ transition of Eu^{3+}.

DOI: 10.1021/acs.chemmater.7b03918
Chem. Mater. 2017, 29, 10122–10129

broad emission of BAM:Eu is indeed the sum of multiple contributions from Eu^{2+} on different crystallographic sites. XRD[31] and Mössbauer spectroscopy[32] investigations on undamaged BAM:Eu and photoluminescence[33] (PL) of BAM:Sm^{2+} established that the lanthanide ion occupies at least three crystallographic sites in the CL: the Beaver−Ross (BR), i.e., the Ba site, the anti-BR (a-BR) and the mid-Oxygen (mO) (Figure 1).[33] Because Eu 5d orbitals are more delocalized than 4f orbitals and more sensitive to the crystal field generated by ligands, the local environment corresponding to each site results in a different Eu^{2+} emission. The redshift occurring during damage is a signature for variations in contributions from luminescent Eu^{2+} in different lattice sites. Interestingly, the redshift and the broadening occur on longer time scales compared to the decrease in intensity as indicated by the time when 63% of the full range of variation is reached (see insets), which is 66 s for the redshift and 18.6 s for the RL intensity. The broadening is even slower and develops on the long wavelength side of the spectrum.

The series of HERFD-XANES collected at the Eu L_3-edge and probing the sample at increasing damage are shown in Figure 4. The L_3-edge spectrum of Eu consists of two intense

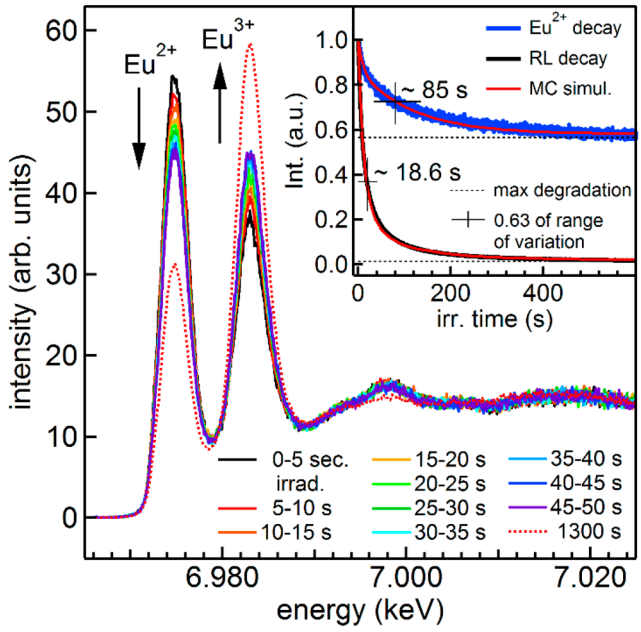

Figure 4. Effects of irradiation on Eu L_3-edge on BAM:Eu. The inset shows the decay of the Eu^{2+} XANES peak during continuous irradiation (blue line) and the decay of the RL intensity (black line). The red lines show the results of the Monte Carlo simulation accounting for the generation of luminescence killer centers along with the oxidation of Eu^{2+} ions.

peaks at 6.975 and 6.983 keV characteristic of Eu^{2+} and Eu^{3+} respectively.[34] The first spectrum of the series presents both peaks indicating that a considerable amount of Eu^{3+} is incorporated in the pristine sample. With progressive irradiation the amount of Eu^{2+} decreases in favor of Eu^{3+}, while in the postedge region no noticeable changes are observed during the first 45 s. A lowering of the postedge feature at 6.998 keV is observed after 1300 s of irradiation. The oxidation of Eu^{2+} as a function of irradiation time was acquired in parallel to RL data presented in Figure 2 and 3 and is shown in the inset of Figure 4 (incident X-ray energy fixed at 6.975 keV). The Eu^{2+} content as detected from XANES decreases to a minimum of 56% of the initial intensity after 1000 s and remains stable for further irradiation. As in the case of the RL redshift, the Eu oxidation is slower than the decrease of luminescence intensity. 63% of the full range of variation is in fact reached after 85 s to be compared with the 18.6 s needed to the RL intensity.

To probe the effects of irradiation on the host lattice we measured HERFD-XANES at Ba L_3-edge on BAM:Eu and at Mn K-edge on BAM:Eu,Mn with the same procedure as that employed for the Eu L_3-edge. The Ba L_3-edge is shown in Figure 5. For comparison with the Eu L_3-edge the energy scale

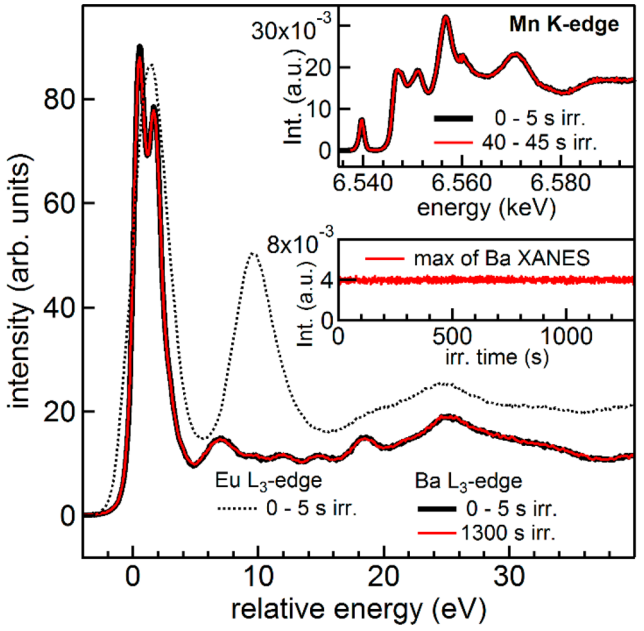

Figure 5. Ba and Eu L_3-edge of fresh and irradiated BAM:Eu. The absorption energies were shifted to bring the maximum of the derivative to zero. Bottom inset shows the intensity of Ba white line maximum measured during continuous irradiation. Top inset shows XANES of Mn K-edge measured on BAM:Eu,Mn corresponding to 0−5 and 40−45 s of irradiation.

was shifted such that the maximum of the first derivative is at 0 eV. The Ba XANES does not show any significant change with increasing X-ray dose. The inset shows the intensity of the Ba white line during 1300 s of continuous irradiation. The postedge of Eu HERFD-XANES recalls the group of features between 16 and 30 eV of Ba HERFD-XANES but broadened. This resemblance is indicative of the similarity of Ba and Eu local atomic environments and suggests that all sites occupied by Eu are similar to the BR site. We note that Eu^{2+} and Eu^{3+} contribute to this region of the spectrum and we conclude that oxidation of Eu^{2+} does not entail a change of its local environment. A mild lowering of this group of features in Eu XANES was actually observed (Figure 4) in the sample irradiated for 1300 s and may be correlated to the migration of a fraction of Eu out of their original site. The top inset of Figure 5 shows Mn K-edge HERFD-XANES which were acquired on codoped samples where Mn^{2+} replaces Mg^{2+} in tetrahedral sites in the spinel block. As for Ba HERFD-XANES no variation was observed with irradiation. The codoped sample was also measured at the Eu L_3-edge and it undergoes the same degradation process observed on BAM:Eu.

DOI: 10.1021/acs.chemmater.7b03918
Chem. Mater. 2017, 29, 10122−10129

The Eu^{2+} atoms oxidized by the X-ray beam can be fully recovered by annealing at moderate temperature in a reducing atmosphere. Figure 6 shows the spectra of the sample that

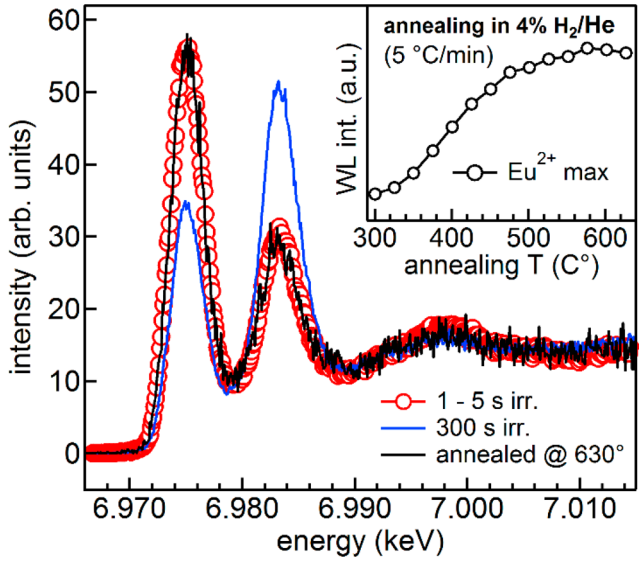

Figure 6. Eu L_3-edge HERFD-XANES spectra of BAM:Eu showing the recovery of Eu^{2+} with annealing. The curves shown were acquired on the same spots of the sample after irradiation with the minimal dose (red-dot curve), irradiation for 300 s (blue line), and annealing to 630 °C in 4% H_2/He atmosphere. The inset shows the progressive increase of Eu^{2+} XANES peak during the annealing process.

received the minimal dose of X-rays, equal to the 5 s of acquisition time, and that of the same sample after 300 s of X-rays irradiation. After irradiation the amount of Eu^{3+} has clearly increased. At this point the sample was annealed in a 4% H_2/He gas mixture to 630 °C maximum temperature. The spectrum acquired after the annealing on the same spot that was previously irradiated shows that the amount of Eu^{2+} is recovered to the initial value at the end of the annealing. During the annealing the intensity of Eu^{2+} peak was regularly sampled (Figure 6, inset) showing that the recovery of Eu^{2+} starts at temperatures as low as 340 °C.

DISCUSSION

The effects of X-ray irradiation on RL spectra are the same as VUV induced damage and manifest themselves in a decrease of intensity, a redshift and a broadening on the long wavelength side of the emission band. The broad emission of BAM:Eu is due to the sum of three contributions from luminescent Eu^{2+} on multiple sites, generally identified in BR, a-BR, and mO sites (Figure 1).[32,33,35,36] From literature the BR site is generally agreed to be the principal emitter, with the characteristic emission peaked at shorter wavelength compared to that of a-BR and mO. The redshift and broadening of PL spectra is commonly ascribed to migration of Eu^{2+} out of BR sites to a-BR and mO, facilitated by the high ion mobility of the CL. Different sites may have different efficiencies of excitation and emission and migration of Eu is also reported to cause the decrease of luminescence intensity.[15]

We correlate the time scale of the decrease of the luminescence intensity with that of redshift and broadening by monitoring the RL following X-ray illumination (Figure 3 and 4). The result clearly indicates different characteristic times, with redshift and broadening being 3.5 and 10 times slower than the decay of RL intensity. If the lowering of intensity was solely the result of Eu migration, then a similar time-dependence should be found for the two variations. The marked difference in characteristic times is an experimental evidence of the more complex process behind degradation.

A fundamental insight is given by HERFD-XANES acquired at the Eu L_3-edge and presented in Figure 4. These data show that in the first 50 s of irradiation a considerable fraction of Eu^{2+} is oxidized while the XANES postedge does not change visibly. We conclude that the XANES data rule out the migration of a significant fraction of Eu ions in the degradation stage that brings the luminescence to 1%. Interestingly, Eu^{2+} oxidation occurs on a similar time scale as the RL redshift, 85 and 66 s, respectively. A faster oxidation of Eu^{2+} in BR sites is compatible with both the redshift, since it changes the distribution of luminescent Eu, and a stable local environment of Eu. We note that XANES was applied in previous studies to evaluate the oxidation of Eu in BAM:Eu[24,37,38] upon thermal damage. A significant oxidation of Eu was often excluded in degradation by VUV illumination based on the absence of characteristic luminescence of Eu^{3+}. It is, however, well documented that the ratio of Eu^{2+} and Eu^{3+} luminescence is not a good indicator of their relative abundance in phosphors.[39] Our luminescence and X-ray data demonstrate that the fraction of Eu^{3+} increases without a corresponding increase of the Eu^{3+} characteristic luminescence. We stress that XANES probes all Eu present in the sample contrary to RL which probes only luminescent impurities.

In reports discussing the degradation of BAM by VUV irradiation, Eu migration out of BR sites and the photogeneration of defects are proposed as the main mechanisms.[15,16,23] Eu oxidation is generally not considered crucial to explain degradation by VUV. Our data encourage one to reconsider the role of Eu oxidation, suggesting that the processes occurring during VUV illumination and degradation by annealing are similar. Interestingly, the Eu^{2+} atoms oxidized by X-rays can be recovered by a moderate annealing in a reducing atmosphere. The reversibility of the $Eu^{2+/3+}$ redox is compatible with oxidation mediated by defects induced by irradiation and combined with high ion mobility of the CL layer. The formation of a stable phase incorporating Eu^{3+} like the magnetoplumbite $EuMgAl_{11}O_{19}$, which is found for annealing at high temperature, can also be excluded in our case.

Oxidation of Eu^{2+} is certainly contributing to the decrease of light emission since each Eu^{2+} becoming Eu^{3+} represents, concerning blue emission, a formerly active center that oxidation renders inactive. However, a completely degraded sample still contains 56% of Eu^{2+} while luminescence is reduced to only 1% of the initial value. From Figure 4 it is clear that luminescence decreases at significantly higher rate than the decrease of Eu^{2+}. Comparing the Eu^{2+} and the RL signal is justified by the fact that the same sample volume is probed in the two cases. RL is excited by the incoming X-ray beam and emanates from the entire excited volume since the host matrix is transparent to visible light. HERFD-XANES signal is collected from the escape volume of the Eu $L\alpha_1$ photons, which for incoming X-rays with energy at the maximum of Eu^{2+} absorption and with Eu concentration of only 7% is practically the full volume penetrated by the incident beam.

Additional contributions may arise from less efficient primary absorption in the host or inhibited host-to-dopant energy transfer. The mechanism of energy transfer to Eu^{2+} impurities

DOI: 10.1021/acs.chemmater.7b03918
Chem. Mater. 2017, 29, 10122−10129

when energy is absorbed in the host matrix is not fully understood. It is known from excitation spectra that both absorption in the Ba−O groups and in the spinel block result in efficient transfer to Eu^{2+}.[10,16,40] The excitation spectrum is in fact flat over a large range of absorption wavelengths that covers absorption in the near gap region[41] (∼6.8 eV, ∼180 nm) where Ba−O groups absorb and in the deep VUV (∼8.5−10.3 eV, ∼145−120 nm) where the spinel block absorbs.[35,42] Absorption of VUV light near the energy gap in undoped BAM results in host-lattice emission that well matches the absorption of Eu^{2+} and is thought to be the main path for host-to-dopant energy transfer. The mechanism of energy transfer when light is absorbed in the spinel block is unclear and it was proposed that high lying Eu states could trap charges excited in this region and mediate the transfer.[15,16,35]

Degradation of the host lattice could reduce the absorption of light in the Ba−O groups, hamper the host lattice emission,[15] or create defects in the spinel block that prevent the transfer of energy to Eu^{2+}.[16] Our measurements at Ba L_3- and Mn K-edge show that the structures of both CL and spinel block stay intact during irradiation and, consequently, the bulk properties of the host lattice are preserved. The recovery of Eu^{2+} in damaged BAM:Eu by annealing in reducing atmosphere confirms that no nonreversible structural damage is induced in the host lattice. We thus propose that fast decrease of the luminescence intensity arises from a reduced luminescence efficiency of the remaining Eu^{2+} correlated with the formation of defects during irradiation. A significant increase of the number of defects uniformly spread over the host material would ultimately be visible in HERFD-XANES spectra as variations of near-edge spectral features. We do not observe such variations for Ba and Mn and the defects must thus be in the vicinity of Eu. The formation of defects in pristine BAM and BAM:Eu has been addressed in literature. It is indeed found that irradiation induces oxygen vacancies and can extract interstitial oxygen in the CL.[43,44] These defects may reach Eu^{2+} impurities, induce Eu oxidation and have an impact on the luminescence behavior of remaining Eu^{2+}.

To grasp if the different dynamics observed for Eu oxidation and RL decrease can indeed be explained by the creation of defect centers killing the luminescence, we performed a kinetic Monte Carlo (MC) simulation that implements this model. We considered a large sublattice of $BaMgAl_{10}O_{17}$ comprising 540 000 Ba atoms, 21 600 of which were substituted with randomly distributed Eu atoms, corresponding to a 4% atomic concentration. The initial amount of Eu^{2+} was extracted from XANES analysis. The fraction of Eu^{3+} which is already present from the beginning is not taken into account since we model the dynamics of the Eu^{2+} oxidation and luminescence quenching. The simulation is divided in two steps: the first aims at reproducing the dynamics of Eu oxidation during irradiation and the second uses the dynamics obtained in the first step as the input to reproduce the RL dynamics. To reproduce the oxidation of Eu^{2+}, three subsets of Eu ions are introduced: a set of stable Eu^{2+} impurities resistant to oxidation and two sets of Eu atoms prone to oxidation with probabilities of 100% and 90%, respectively. The need of at least two oxidation probabilities to simulate the experimental data is suggested by the shape of the experimental Eu^{2+} decay that cannot be fitted by a single exponential (Figure 4). In this framework X-ray irradiation is simulated by random events at different domains of the lattice. Any time a Eu^{2+} is found in the domain of an X-ray event, it responds according to the set it belongs to, i.e., oxidizing with a certain probability or remaining divalent. The distribution of Eu in the three subsets was tuned to minimize the difference between the experimental and simulated Eu^{2+} decay curves and the resulting oxidation dynamics was then used as input to simulate the RL behavior. An interaction distance is introduced to generate a quenching sphere around each Eu^{3+} ion that is created upon irradiation. Any Eu^{2+} falling in the quenching sphere of a Eu^{3+} ion can either decay radiatively with decreased quantum efficiency or be quenched completely. At every MC step, an X-ray event occurs after which the number of radiatively decaying and quenched Eu^{2+} ions are counted. In this way the decrease of RL intensity is the combination of the formation of Eu^{3+} and the decreased efficiency of the Eu^{2+} surrounding it.

The results of the simulation are superimposed to the experimental data in the inset of Figure 4. The times in which only a fraction of 1/e of nonoxidized Eu^{2+} is left for the two subsets are found to be 14 and 120 s, for the sets with 100% and 90% probability of oxidation, respectively. The good agreement indicates that this simple model succeeds in accurately reproducing the quenching of the RL as correlated to the oxidation process. The proposed mechanism, i.e., the generation of killer centers along with oxidation of Eu, can account for the accelerated decrease of RL intensity. The radius of the quenching sphere to obtain the final result was 24 Å, meaning that the interaction between Eu^{2+} and killer centers is not restricted to the same CL, but can span neighboring CLs. Deliberately changing the other fitting parameters in the simulation did not significantly affect the interaction distance. It would be interesting to extend this combined X-ray degradation and radioluminescence study to BAM phosphors with a wide range of europium concentration, as this should have an effect on the degradation speed.

Our results suggest that improving the stability of Eu^{2+} in the host lattice is a first viable path to strengthen BAM:Eu against irradiation. More Eu^{2+} atoms would survive irradiation, increasing the probability of radiative emission. In addition, even if the nature of the defects that quench the luminescence of the remaining Eu^{2+} is yet to be clarified, it is likely connected to Eu^{2+} oxidation as suggested by our simple Monte Carlo model and an improved stability of Eu^{2+} may also reduce the formation of the killer centers. Some recent works reported improved stability of BAM:Eu after S-doping or substitution of Al−O bonds close to the CL with Al−N or Si−N groups[45−47] while previous investigations on similar systems found that no improvement is achieved when N is incorporated in the spinel block.[48] Substitution of one Eu−O bond with a Eu−N bond reduces the probability of Eu^{2+} oxidation due to the reduced electronegativity of N and the substitution of O in the CL with S may hamper the formation of vacancies during irradiation.

■ CONCLUSIONS

The original, integrated approach that uses X-rays to simultaneously damage, probe, and excite the sample provides new insight into the degradation process of BAM:Eu. The host lattice, probed through Ba L_3- and Mn K-edge HERFD-XANES, was found to be stable under irradiation while we observed that a significant fraction of Eu^{2+} is oxidized during the degradation process. We ruled out the possibility that migration of Eu ions out of BR sites is the cause of the degradation, and we propose that the redshift and broadening observed on RL are due to preferential oxidation of luminescent Eu^{2+} in BR sites.

DOI: 10.1021/acs.chemmater.7b03918
Chem. Mater. 2017, 29, 10122−10129

The different time scales of RL intensity decay and Eu^{2+} oxidation and the presence of resistant Eu^{2+} indicate that oxidation cannot be the sole reason for the degradation of luminescence intensity. We propose that irradiation induces both Eu^{2+} oxidation and the creation of nonradiative decay channels. A simple Monte Carlo simulation shows that such a combined effect, i.e., the removal of luminescent Eu^{2+} together with the quenching of the remaining Eu^{2+} ions, can account for the experimental observations. The luminescence killer centers that are responsible for this quenching are presumably defects created along with the Eu^{2+} oxidation. Some authors proposed that in the CL oxygen vacancies can form and interstitial oxygens can be liberated during irradiation. These species could act as oxidizing agent and also alter the luminescence behavior of remaining Eu^{2+}. This is a plausible explanation since the bulk properties of the host materials are unchanged during damage.

AUTHOR INFORMATION

Corresponding Authors

*E-mail: lucia.amidani@esrf.fr (L.A.).
*E-mail: philippe.smet@ugent.be (P.F.S.).
*P. Glatzel, e-mail: pieter.glatzel@esrf.fr.

ORCID

Lucia Amidani: 0000-0003-2234-4173
Katleen Korthout: 0000-0003-4353-8620
Jonas J. Joos: 0000-0002-7869-2217
Marte van der Linden: 0000-0002-4085-0320
Heleen F. Sijbom: 0000-0001-6565-9859
Andries Meijerink: 0000-0003-3573-9289
Philippe F. Smet: 0000-0003-4789-5799

Notes

The authors declare no competing financial interest.

ACKNOWLEDGMENTS

The authors would like to thank T. Bohdan for the technical support during experiments on ID26, all the staff of ID26, and M. Moretti, M. Retegan and M. Rovezzi for very fruitful discussions.

REFERENCES

(1) Ronda, C. R. Recent Achievements in Research on Phosphors for Lamps and Displays. *J. Lumin.* **1997**, *72*−*74*, 49−54.
(2) Kim, C.-H.; Kwon, I.-E.; Park, C.-H.; Hwang, Y.-J.; Bae, H.-S.; Yu, B.-Y.; Pyun, C.-H.; Hong, G.-Y. Phosphors for Plasma Display Panels. *J. Alloys Compd.* **2000**, *311* (1), 33−39.
(3) Toda, K. Recent Research and Development of VUV Phosphors for a Mercury-Free Lamp. *J. Alloys Compd.* **2006**, *408*−*412*, 665−668.
(4) Wang, Z. L.; Cheah, K. W.; Tam, H. L.; Gong, M. L. Near-Ultraviolet Light Excited Deep Blue-Emitting Phosphor for Solid-State Lighting. *J. Alloys Compd.* **2009**, *482* (1−2), 437−439.
(5) Shen, C.; Yang, Y.; Jin, S.; Ming, J. Luminous Characteristics and Thermal Stability of $BaMgAl_{10}O_{17}:Eu^{2+}$ Phosphor for White Light-Emitting Diodes. *Phys. B* **2010**, *405* (4), 1045−1049.
(6) Shen, C.; Yang, Y.; Jin, S.; Ming, J.; Feng, H.; Xu, Z. White Light-Emitting Diodes Using Blue and Yellow-Orange-Emitting Phosphors. *Optik* **2010**, *121* (16), 1487−1491.
(7) Lin, C. C.; Liu, R.-S. Advances in Phosphors for Light-Emitting Diodes. *J. Phys. Chem. Lett.* **2011**, *2* (11), 1268−1277.
(8) Smet, P. F.; Parmentier, A. B.; Poelman, D. Selecting Conversion Phosphors for White Light-Emitting Diodes. *J. Electrochem. Soc.* **2011**, *158* (6), R37−R54.
(9) Pradal, N.; Potdevin, A.; Chadeyron, G.; Bonville, P.; Caillier, B.; Mahiou, R. Spectroscopic Study and Enhanced Thermostability of Combustion-Derived $BaMgAl_{10}O_{17}:Eu^{2+}$ Blue Phosphors for Solid-State Lighting. *Opt. Mater.* **2017**, *64*, 334−344.
(10) Jüstel, T.; Lade, H.; Mayr, W.; Meijerink, A.; Wiechert, D. U. Thermoluminescence Spectroscopy of Eu^{2+} and Mn^{2+} Doped $BaMgAl_{10}O_{17}:Eu^{2+}$. *J. Lumin.* **2003**, *101* (3), 195−210.
(11) Jüstel, T.; Krupa, J.-C.; Wiechert, D. U. VUV Spectroscopy of Luminescent Materials for Plasma Display Panels and Xe Discharge Lamps. *J. Lumin.* **2001**, *93* (3), 179−189.
(12) Oshio, S.; Matsuoka, T.; Tanaka, S.; Kobayashi, H. Mechanism of Luminance Decrease in $BaMgAl_{10}O_{17}:Eu^{2+}$ Phosphor by Oxidation. *J. Electrochem. Soc.* **1998**, *145* (11), 3903−3907.
(13) Bizarri, G.; Moine, B. On $BaMgAl_{10}O_{17}:Eu^{2+}$ Phosphor Degradation Mechanism: Thermal Treatment Effects. *J. Lumin.* **2005**, *113* (3−4), 199−213.
(14) Lacanilao, A.; Wallez, G.; Mazerolles, L.; Dubot, P.; Binet, L.; Pavageau, B.; Servant, L.; Buissette, V.; Le Mercier, T. Structural Analysis of Thermal Degradation and Regeneration in Blue Phosphor $BaMgAl_{10}O_{17}:Eu^{2+}$ Based upon Cation Diffusion. *Solid State Ionics* **2013**, *253*, 32−38.
(15) Howe, B.; Diaz, A. L. Characterization of Host-Lattice Emission and Energy Transfer in $BaMgAl_{10}O_{17}:Eu^{2+}$. *J. Lumin.* **2004**, *109* (1), 51−59.
(16) Dawson, B.; Ferguson, M.; Marking, G.; Diaz, A. L. Mechanisms of VUV Damage in $BaMgAl_{10}O_{17}:Eu^{2+}$. *Chem. Mater.* **2004**, *16* (25), 5311−5317.
(17) Bizarri, G.; Moine, B. On $BaMgAl_{10}O_{17}:Eu^{2+}$ Phosphor Degradation Mechanism by Vacuum-Ultraviolet Excitation. *J. Appl. Phys.* **2005**, *98* (11), 113528−1.
(18) Yeh, C.-W.; Chen, W.-T.; Liu, R.-S.; Hu, S.-F.; Sheu, H.-S.; Chen, J.-M.; Hintzen, H. T. Origin of Thermal Degradation of $Sr_{2-x}Si_5N_8:Eu_x$ Phosphors in Air for Light-Emitting Diodes. *J. Am. Chem. Soc.* **2012**, *134* (34), 14108−14117.
(19) Iyi, N.; Inoue, Z.; Kimura, S. The Crystal Structure and Cation Distribution of Highly Nonstoichiometric Magnesium-Doped Potassium b-Alumina. *J. Solid State Chem.* **1986**, *61*, 236−244.
(20) Yang, P.; Yao, G.-Q.; Lin, J.-H. Energy Transfer and Photoluminescence of $BaMgAl_{10}O_{17}:Eu^{2+}$ Co-Doped with Eu^{2+} and Mn^{2+}. *Opt. Mater.* **2004**, *26* (3), 327−331.
(21) Zhang, S.; Kokubu, M.; Fujii, H.; Uchiike, H. A Study on the Chromaticity Shifts of Blue Phosphor for Color Plasma Displays. *J. Soc. Inf. Disp.* **2002**, *10* (1), 25−29.
(22) Zhang, S.; Kono, T.; Ito, A.; Yasaka, T.; Uchiike, H. Degradation Mechanisms of the Blue-Emitting Phosphor $BaMgAl_{10}O_{17}:Eu^{2+}$ under Baking and VUV-Irradiating Treatments. *J. Lumin.* **2004**, *106* (1), 39−46.
(23) Zhang, J.-C.; Zhou, M.-J.; Wang, Y.-H. Photoluminescence Degradation Mechanism of $BaMgAl_{10}O_{17}:Eu^{2+}$ Phosphor by Vacuum Ultraviolet Irradiation. *Chin. Phys. B* **2012**, *21* (12), 124102−1.
(24) Hirosawa, I.; Honma, T.; Kato, K.; Kijima, N.; Shimomura, Y. Influence of X-Ray Irradiation on Doped Europium in $BaMgAl_{10}O_{17}:Eu^{2+}$ Studied by X-Ray Absorption Fine Structure and X-Ray Diffraction. *J. Soc. Inf. Disp.* **2005**, *13* (8), 673−678.
(25) Zhang, J.; Zhou, M.; Liu, B.; Wen, Y.; Wang, Y. The Ultraviolet Irradiation Degradation of Fluorescent Lamp Used $BaMgAl_{10}O_{17}:Eu^{2+},Mn^{2+}$ Phosphor. *J. Lumin.* **2012**, *132* (8), 1949−1952.
(26) Gauthier, C.; Solé, V. A.; Signorato, R.; Goulon, J.; Moguiline, E. The ESRF Beamline ID26: X-Ray Absorption on Ultra Dilute Sample. *J. Synchrotron Radiat.* **1999**, *6* (3), 164−166.
(27) Glatzel, P.; Weng, T.-C.; Kvashnina, K.; Swarbrick, J.; Sikora, M.; Gallo, E.; Smolentsev, N.; Mori, R. A. Reflections on Hard X-Ray Photon-in/Photon-out Spectroscopy for Electronic Structure Studies. *J. Electron Spectrosc. Relat. Phenom.* **2013**, *188*, 17−25.
(28) Galajev, S. Degradation Process in $BaMgAl_{10}O_{17}:Eu^{2+}$ and $BaMgAl_{14}O_{23}:Eu^{2+}$. Master's Thesis; Tartu University: Tartu, Estonia, 2008.
(29) Kim, Y.; Kang, S. Investigation of the Degradation Mechanisms in $BaMgAl_{10}O_{17}:Eu^{2+}$ Phosphor: On the Influence of Thermal Process on Operational Durability. *Appl. Phys. B: Lasers Opt.* **2010**, *98* (2−3), 429−434.

DOI: 10.1021/acs.chemmater.7b03918
Chem. Mater. 2017, 29, 10122−10129

(30) Wang, X.; Li, J.; Shi, P.; Guan, W.; Zhang, H. High Dispersibility and Enhanced Luminescence Properties of $BaMgAl_{10}O_{17}:Eu^{2+}$ Phosphors Derived from Molten Salt Synthesis. *Opt. Mater.* **2015**, *46*, 432−437.
(31) Lambert, J.; Wallez, G.; Quarton, M.; Le Mercier, T.; van Beek, W. Searching for the Dopant Ion in Eu^{2+}-Activated $BaMgAl_{10}O_{17}:Eu^{2+}$ Phosphor with Synchrotron Diffraction. *J. Lumin.* **2008**, *128* (3), 366−372.
(32) Boolchand, P.; Mishra, K. C.; Raukas, M.; Ellens, A.; Schmidt, P. C. Occupancy and Site Distribution of Europium in Barium Magnesium Aluminate by ^{151}Eu Mössbauer Spectroscopy. *Phys. Rev. B: Condens. Matter Mater. Phys.* **2002**, *66* (13), 134429.
(33) Ellens, A.; Zwaschka, F.; Kummer, F.; Meijerink, A.; Raukas, M.; Mishra, K. Sm^{2+} in BSM: Fluorescent Probe for the Number of Luminescing Sites of Eu^{2+} in BAM. *J. Lumin.* **2001**, *93*, 147−153.
(34) Röhler, J.. Chapter 71. In *Handbook on the Physics and Chemistry of Rare Earths*; Gschneidner, K. A. J., Eyring, L., Hüfner, S., Eds.; Elsevier Science Publishers B.V.: Amsterdam, 1987; Vol. *10*, pp 453−545.
(35) Mishra, K. C.; Raukas, M.; Ellens, A.; Johnson, K. H. A Scattered Wave Model of Electronic Structure of Eu^{2+} in $BaMgAl_{10}O_{17}:Eu^{2+}$ and Associated Excitation Processes. *J. Lumin.* **2002**, *96* (2), 95−105.
(36) Pike, V.; Patraw, S.; Diaz, A. L.; DeBoer, B. G. Defect Chemistry and VUV Optical Properties of the $BaMgAl_{10}O_{17}:Eu^{2+}$-$BaAl_{0.75\ 11}O_{17.25}:Eu^{2+}$ Solid Solution. *J. Solid State Chem.* **2003**, *173* (2), 359−366.
(37) Kim, K.-B.; Kim, Y.-I.; Chun, H.-G.; Cho, T.-Y.; Jung, J.-S.; Kang, J.-G. Structural and Optical Properties of $BaMgAl_{10}O_{17}:Eu^{2+}$ Phosphor. *Chem. Mater.* **2002**, *14* (12), 5045−5052.
(38) Sohn, K.-S.; Kim, S. S.; Park, H. D. Luminescence Quenching in Thermally-Treated Barium Magnesium Aluminate Phosphor. *Appl. Phys. Lett.* **2002**, *81* (10), 1759−1761.
(39) Avci, N.; Korthout, K.; Newton, M. A.; Smet, P. F.; Poelman, D. Valence States of Europium in $CaAl_2O_4$:Eu Phosphors. *Opt. Mater. Express* **2012**, *2* (3), 321−330.
(40) Yoshida, H.; Yamazaki, T.; Toyoshima, H.; Watanabe, S.; Ogasawara, K.; Yamamoto, H. Experimental and Theoretical Investigations for Excitation Properties of $Ba_{1-x}Eu_xMgAl_{10}O_{17}$. *J. Electrochem. Soc.* **2007**, *154* (7), J196−J200.
(41) Lushchik, A.; Lushchik, C.; Feldbach, E.; Kudryavtseva, I.; Liblik, P.; Maaroos, A.; Nagirnyi, V.; Savikhin, F.; Vasil'chenko, E. Photon Multiplication in Wide-Gap BAM and SAM Aluminates. In *Proceedings of SPIE*; Rosental, A., Ed.; Tartu, 2005; Vol. *5946*, pp 594609−1−12.
(42) Onuma, H.; Yamashita, I.; Serizawa, K.; Tanno, H.; Suzuki, A.; Tsuboi, H.; Hatakeyama, N.; Endou, A.; Takaba, H.; Kubo, M.; Kajiyama, H.; Miyamoto, A. Quantum Chemistry and QSPR Study on Relationship between Crystal Structure and Emission Wavelength of Eu^{2+}-Doped Phosphors. *J. Soc. Inf. Disp.* **2010**, *18* (4), 301−309.
(43) Wu, Z.; Cormack, A. N. Defects in $BaMgAl_{10}O_{17}:Eu^{2+}$ Blue Phosphor. *J. Electroceram.* **2003**, *10* (3), 179−191.
(44) Gourier, D.; Gbehi, T.; Visocekas, R.; Thery, J.; Vivien, D. Color Centres in Barium Hexaaluminate (Phase I) Studied by Electron Paramagnetic Resonance, Optical Absorption, and Thermally Stimulated Luminescence. *Phys. Status Solidi B* **1989**, *152*, 415−429.
(45) Liu, B.; Wang, Y.; Zhang, F.; Wen, Y.; Dong, Q.; Wang, Z. Thermal Stability and Photoluminescence of S-Doped $BaMgAl_{10}O_{17}:Eu^{2+}$ Phosphors for Plasma Display Panels. *Opt. Lett.* **2010**, *35* (18), 3072−3074.
(46) Wang, Y.-F.; Wang, Y.-F.; Zhu, Q.-Q.; Hao, L.-Y.; Xu, X.; Xie, R.-J.; Agathopoulos, S. Luminescence and Structural Properties of High Stable Si-N-Doped $BaMgAl_{10}O_{17}:Eu^{2+}$ Phosphors Synthesized by a Mechanochemical Activation Route. *J. Am. Ceram. Soc.* **2013**, *96* (8), 2562−2569.
(47) Wang, Y.; Tang, J.; Ouyang, X.; Liu, B.; Lin, R. H. Photoluminescence Properties of AlN-Doped $BaMgAl_{10}O_{17}:Eu^{2+}$ Phosphors. *Mater. Res. Bull.* **2013**, *48* (6), 2123−2127.
(48) Jansen, S. R.; Migchels, J. M.; Hintzen, H. T.; Metselaar, R. Eu-Doped Barium Aluminum Oxynitride with the β-Alumina-Type Structure as New Blue-Emitting Phosphor. *J. Electrochem. Soc.* **1999**, *146* (2), 800−806.

DOI: 10.1021/acs.chemmater.7b03918
Chem. Mater. 2017, 29, 10122−10129